Front. Struct. Civ. Eng. 2016, 10(2): 214–223
DOI 10.1007/s11709-016-0332-3

RESEARCH ARTICLE

The effect of carbon nanotubes and polypropylene fibers on bond of reinforcing bars in strain resilient cementitious composites

Souzana P. TASTANI*, Maria S. KONSTA-GDOUTOS, Stavroula J. PANTAZOPOULOU, Victor BALOPOULOS

Department of Civil Engineering, Democritus University of Thrace, Vas. Sofias Street, #12 Xanthi 67100, Greece
**Corresponding author. E-mail: stastani@civil.duth.gr*

ABSTRACT Stress transfer between reinforcing bars and concrete is engaged through rib translation relative to concrete, and comprises longitudinal bond stresses and radial pressure. The radial pressure is equilibrated by hoop tension undertaken by the concrete cover. Owing to concrete's poor tensile properties in terms of strength and deformability, the equilibrium is instantly released upon radial cracking of the cover along the anchorage with commensurate abrupt loss of the bond strength. Any improvement of the matrix tensile properties is expected to favorably affect bond in terms of strength, resilience to pullout slip, residual resistance and controlled slippage.The aim of this paper is to investigate the local bond of steel bars developed in adverse tensile stress conditions in the concrete cover. In the tests, the matrix comprises a novel, strain resilient cementitious composite (SRCC) reinforced with polypropylene fibers (PP) with the synergistic action of carbon nano-tubes (CNT). Local bond is developed over a short anchorage length occurring in the constant moment region of a four-point bending short beam. Parameters of investigation were the material structure (comprising a basic control mix, reinforced with CNTs and/or PP fibers) and the age of testing. Accompanying tests used to characterize the cementitious material were also conducted. The test results illustrate that all the benefits gained due to the synergy between PP fibers and CNTs in the matrix, namely the maintenance of the multi-cracking effect with time, the increased strength and deformability as well as the highly increased material toughness, were imparted in the recorded bond response. The local bond response curves thus obtained were marked by a resilient appearance exhibiting sustained strength up to large levels of controlled bar-slip; the elasto-plastic bond response envelope was a result of the confining synergistic effect of CNTs and the PP fibers, and it occurred even without bar yielding.

KEYWORDS carbon nanotubes, strain resilient cementitious composite, polypropylene fibers, tensile bending, bond

1 Introduction

In conventional reinforced concrete, bar-slip represents the relative translation of the reinforcing bar ribs with respect to the surrounding media. During bar-pullout the translating ribs exert significant radial pressures on the cover (σ_n, in Fig. 1), at the bar-concrete boundary. This is the radial component of the bond mechanism, which is equilibrated by concrete hoop tensile stresses (σ_{hoop} in Fig. 1). Radial cracking develops when hoop stresses exceed the tensile strength of the cover material; at that point, bar-concrete interaction is released instantaneously. Upon cover cracking, the bond stresses, i.e., the longitudinal shear stresses at the bar-concrete interface are released, and the bond strength is lost, whereas the bar begins to slip uninhibited. This is reflected in the local bond-slip relationship that characterizes the interaction at the interface between the two materials, by the post-peak descending branch [1,2].

To eliminate the brittle nature of the bond-slip law which is observed in conventional concretes, a strain resilient cementitious composite (SRCC) with a high tensile strain capacity and improved tensile strength is considered as the host matrix. The ductility and resilience of this innovative cementitious material provides an interesting test-bed for

Article history: Received Apr 17, 2015; Accepted Dec 19, 2015

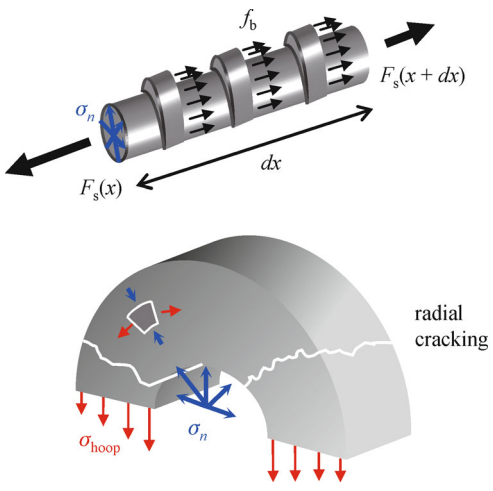

Fig. 1 Bond shear stresses f_b along an elementary segment and radial stresses σ_n sustained by hoop media stresses σ_{hoop}

the development of bond and stress-transfer [3], since transverse tensile strength in the bar-cover is sustained up to large hoop strains due to the bridging effect provided by the fibers [4,5] and the fine-grained matrix often enhanced by nano-materials.

Available tests on CNT and fiber-reinforced cementitious mortars [6,7] illustrate that whereas micro-fibers ameliorate the strain capacity in tension, the CNTs impart significantly higher energy for crack propagation and thus increased tensile strength, by arresting the propagation of cracks at the nanoscale in the matrix structure. These effects are expected to favorably affect the matrix-to-reinforcement bond strength, although tests verifying this assumption are still not available.

Few experimental investigations have been published regarding the bond-slip behavior of deformed steel bars embedded in fine-grained fiber reinforced cementitious composites, even without nano-additives. Chao et al. [8] conducted modified-pullout tests, where both the pulled bar and the surrounding media are stressed in tension along the anchorage length L_b (this is a prerequisite condition of the test setup so that the SRCC matrix may be able to develop its enhanced ductility in tension). It was observed that the large deformation capacity of the bar cover enables a much milder descend in the post-peak branch of the bond-slip law regulating accordingly the deformation capacity of reinforced concrete anchorages. In this modified pullout test the matrix hoop tensile stress was varied along the anchorage length; thus the intensity of multi-cracking was accordingly hampered. Bandelt and Billington [4,5] conducted splice tests, thus securing constant hoop tensile stress of the matrix lengthwise along the splice zone; they measured similar bond response, but smaller magnitudes than Chao et al. [8] due to longer embedded length and the nature of the bond mechanism (splice versus anchorage).

The aim of the experimental effort presented herein was to explore the effect that the tensile strain capacity of a strain resilient cementitious matrix would have on the bond mechanism and the strain development capacity of embedded reinforcement. The latter is the ultimate strain the reinforcement would be able to develop given its anchorage length. The mix comprised fine-grained particles and was reinforced with carbon nano-tubes (CNT) and micro polypropylene fibers (PP). With reference to the strain ductility of the matrix, the age of testing is critical because the gradual strength increase seems to compromise debonding and pull out of fibers in favor of strain localization and eventual failure by fiber rupture [9,10]; thus age of testing is a variable of the experimental program (dates of testing 30 and 70 d after casting).

For the purpose of investigating bond of reinforcement embedded in the proposed cementitious matrix, a novel test was developed where local bond is studied in the constant moment region of a short beam in four-point bending, with the bar anchorage occurring in the tension side of the specimen. Thus, along the anchorage length L_b of the studied bond, (where $L_b = 5D_b$, D_b is the diameter equal to 10 mm of a steel bar with yielding stress $f_y = 500$ MPa and modulus of Elasticity $E_s = 200$ GPa) both reinforcement and matrix are highly mobilized in tension, and as such their tensile properties influence the measured average bond-slip law. The experimental program consisted of twelve beam specimens. Parameter of study in the experimental program was the distributed reinforcement of the matrix structure which imparts its resilience in tension. Thus, four variations of the basic matrix were considered, namely, (i) the control matrix, (ii) the control matrix reinforced with CNTs (both of those did not contain other fibers); (iii) the SRCC material comprising the control matrix (i) reinforced with PP fibers, and (iv) the SRCC material used in (iii) enhanced by the addition of CNTs. For each one of the matrices considered, an additional set of three prism samples (40 mm × 40 mm × 160 mm) were also tested in three-point bending for measuring the relevant flexural tensile response at the same age of the associated bond specimens for better correlation of the results.

2 Matrix characteristics

The design of the cementitious matrix was initially based on a former study [9] in light of the requirements for achieving a material that during casting does not require any additional vibration or consolidation even after the addition of the PP fibers and/or the CNTs. In the present investigation the mix design denoted as M1 was modified slightly without altering the mixing ratios [9]. Modifications concerned two ingredients: (a) calcareous fly ash with high content of free lime (CaO_f in the order of 13%) was

used instead of type F fly ash; (b) the size of the PP fibers had an aspect ratio of ℓ_f/d_f = 12 mm/25 μm = 480, i.e., higher than the original ℓ_f/d_f = 8 mm/20 μm = 400. These alterations were dictated by the local availability of these two materials. The second mix (denoted as M2 in Table 1) was appropriately adjusted by reducing the fly ash ratio and increasing the PP fiber-content in order to achieve a longer range of strain resilience by maintaining the water to fine particles ratio identical to the M1.

Prior to the addition of PP fibers both mixes were clearly very flowable, but flowability was compromised as soon as fibers were slowly added to the mix (Fig. 2(a)). To improve the distribution of fibers, a high dosage of high range water reducer (HRWR by SIKA, see Table 1) was needed, which however did not induce any bleeding or segregation due to the fine-grained ingredients and the absence of coarse aggregates. At this preparatory stage, where the appropriateness of the altered materials in terms of mix content was the issue of study, the use of CNTs, being a high-cost material, was not mandatory. The density of the M2 mix was estimated as 1949 kg/m^3 (or 1970 kg/m^3 without the PP) based on the constituent materials (ρ_c = 3.1, ρ_{FA} = 2.6, ρ_{sand} = 2.6, ρ_{PP} = 0.91 in g/cm^3); the addition of CNTs did not alter these values owing to its limited dosage in the mix (0.1 wt% by cement weight).

Figure 2(a) illustrates the state of the fresh mixtures before and after the addition of the fibers, whereas Fig. 2(b) shows the failure modes (cracking pattern) of the associated 40 mm×40 mm×160 mm prisms tested in 3-point bending after 14 d of moist-curing. Figure 3 presents average envelopes of three prisms of each mixture. Clearly the M2 prisms developed a more resilient response to tension than the M1 tests marked by multiple cracking in the zone of high flexural moment (Fig. 2(b)) and strain-resilience in tension up to higher deflection levels (Fig. 3). For these reasons the M2 mix was chosen as the appropriate matrix for the subsequent tests.

The CNTs used in the M2 of the main experimental program were multi-walled carbon nanotubes (MWCNTs by Glonatech, ONEX 1000C) with an average aspect ratio close to 500 (i.e., ℓ_{CNT}/d_{CNT} = 10 μm/20 nm = 500). Since CNTs tend to aggregate due to Van der Waals forces, effective dispersion was achieved by applying ultrasonic energy of 2800 J/lt [11,12] to an aqueous surfactant solution of CNTs and HRWR (HRWR by SIKA, trade name Viscocrete Ultra 600) with mix proportion per weight as CNT:HRWR:water = 1:4:300 (1 part of CNTs, 4 parts of HRWR and 300 parts of water, parts expressed per weight). The sonicator was operated at an amplitude of 50% so as to deliver constant energy rate of 1900−2100 J/min, in cycles of 20 s in order to prevent overheating of the suspensions. Based on previous research [6], the optimum dosage of CNTs in the M2 mix was set to 0.1 wt% by weight of cement.

2.1 Mechanical properties of the matrices

The 40 mm × 40 mm × 160 mm prisms were tested in 3-point bending (clear span of 140 mm) under displacement control with a loading rate of 0.1 mm/min; tests were

Table 1 Mix designation

mix design	portl. cem., 42.5	fine fly ash	fine sand (d_{agg} < 0.5 mm)	water	HRWR[a)]	PP[b)] (vol.)
M1	1	2.8	1.12	1.4 (0.368)[c)]	0.09	1.5%
M2	1	2	1.1	1.1 (0.366)[c)]	0.1	2%

[a)] High range water reducer (SIKA, Viscocrete Ultra 600). [b)] PP fibers (ThracePlastics, TMIX-12): d_f = 25 μm, ℓ_f = 12 mm, f_{fu} = 400 MPa, E_f = 1.6 GPa, ρ_f = 0.91 gr/cm^3, hydrophobic. [c)] water/cement & fly ash
Note: apart from the PP fibers values which are given as volume fractions of the total mix, all other quantities are given as multiples of the cement weight

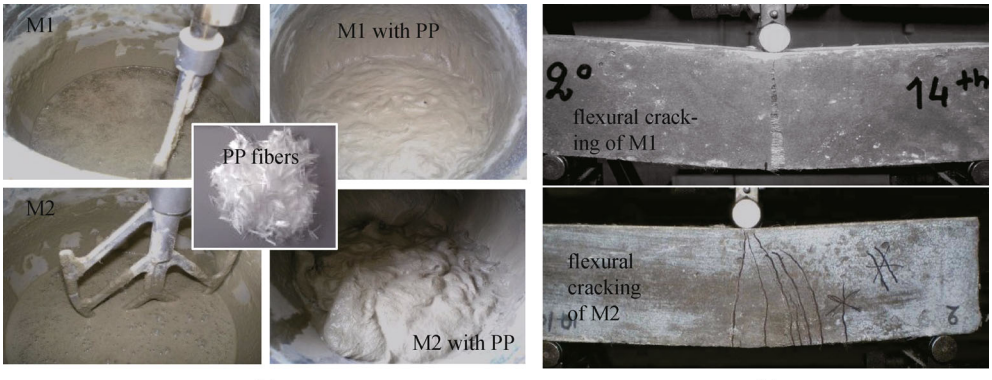

(a) (b)

Fig. 2 Comparative representation of the tested mixtures M1 and M2 regarding (a) the fresh state and (b) the cracking pattern of the associated 3-point bending samples

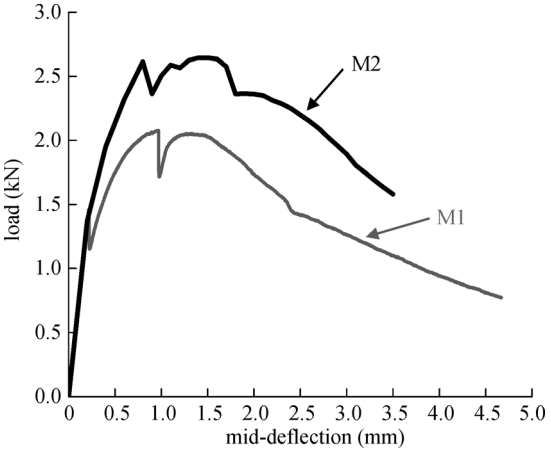

Fig. 3 Average load- deflection histories of the 3-point bending prims of M1 and M2 mixtures

extended up to failure for specimens comprising the control, and the control with CNTs batches. In the case of the SRCC and SRCC-CNT specimens, after the attainment of strength the loading rate was switched to 0.5 mm/min up to at least 50% loss of strength. Figures 4 and 5 present comparative information on the mechanical response of the four batches:

(i) From Fig. 4(a), the addition of the CNTs results in an increase of strength (P_{max}) by as much as 65%; the modulus of rupture (defined as per [13], $f_{t,fl} = 1.5P_{max} \cdot L/(bh^2)$, where $b = h = 40$ mm and $L = 140$ mm), was calculated as 4.75 MPa for the control and 7.83 MPa for the control with CNTs matrix (the term P_{max} used in the calculations of $f_{t,fl}$ is the average maximum load of the group of three tested samples). The apparent flexural toughness of these matrices G_f, quantified by the area enclosed by the envelope and the abscissa divided by the whole cross section area, was found equal to 73 $Nt \cdot m^{-1}$ and 172 $Nt \cdot m^{-1}$ respectively (again G_f, is the average value of three tested samples). Figure 4(b) shows the fractured surface of the control and the control with CNTs prisms after failure. Considering that during casting of the fresh cementitious composite no vibration energy or other consolidation means were used, the fractured surface is notably dense.

(ii) Figures 5(a,b) depict average load versus mid-deflection histories of three prisms of the SRCC and SRCC-CNT mixtures. Figure 5(c) comparatively presents the average envelopes of the SRCC and SRCC-CNT matrices at both ages, from which it is concluded that the addition of PP fibers results in an increase of both the strength and deformation capacity of the SRCC batches as compared to the control batch (in Fig. 4(a)), with these properties further enhanced by the addition of the CNTs (in Fig. 5(c), compare the black and grey curves). Note that the multi-cracking characteristic at the zone of high tensile stresses (see Fig. 5(d)) is recognized by the several jumps in the load — deflection diagrams (in Figs. 5(a,b): every time a new orthogonal crack initiated, a small drop of load occurred to be recovered upon further increase of imposed deformation. For the SRCC matrix (Fig. 5(a)), it may be concluded that the multi-cracking characteristic disappeared as it was tested at a later age (70 d instead of 30 d, see snapshots at left in Fig. 5(d)). This is attributed to increased bonding of fibers in the matrix with age thus altering the deformation pattern of the individual fibers: from controlled pullout which led to distributed cracking in the early stage (i.e., at 30 d), to bond increase with age (this has been also reported in [9]). At 70 d the bond was strong enough to render fibers the most compliant component of

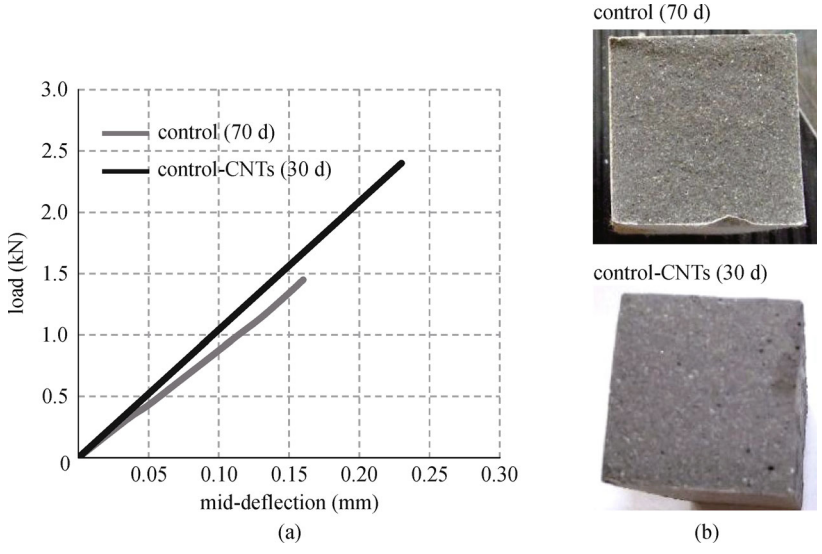

Fig. 4 Control and control with CNTs matrices: (a) average load – mid deflection envelopes of the 3-point bending tests on prims and (b) associated fractured surfaces

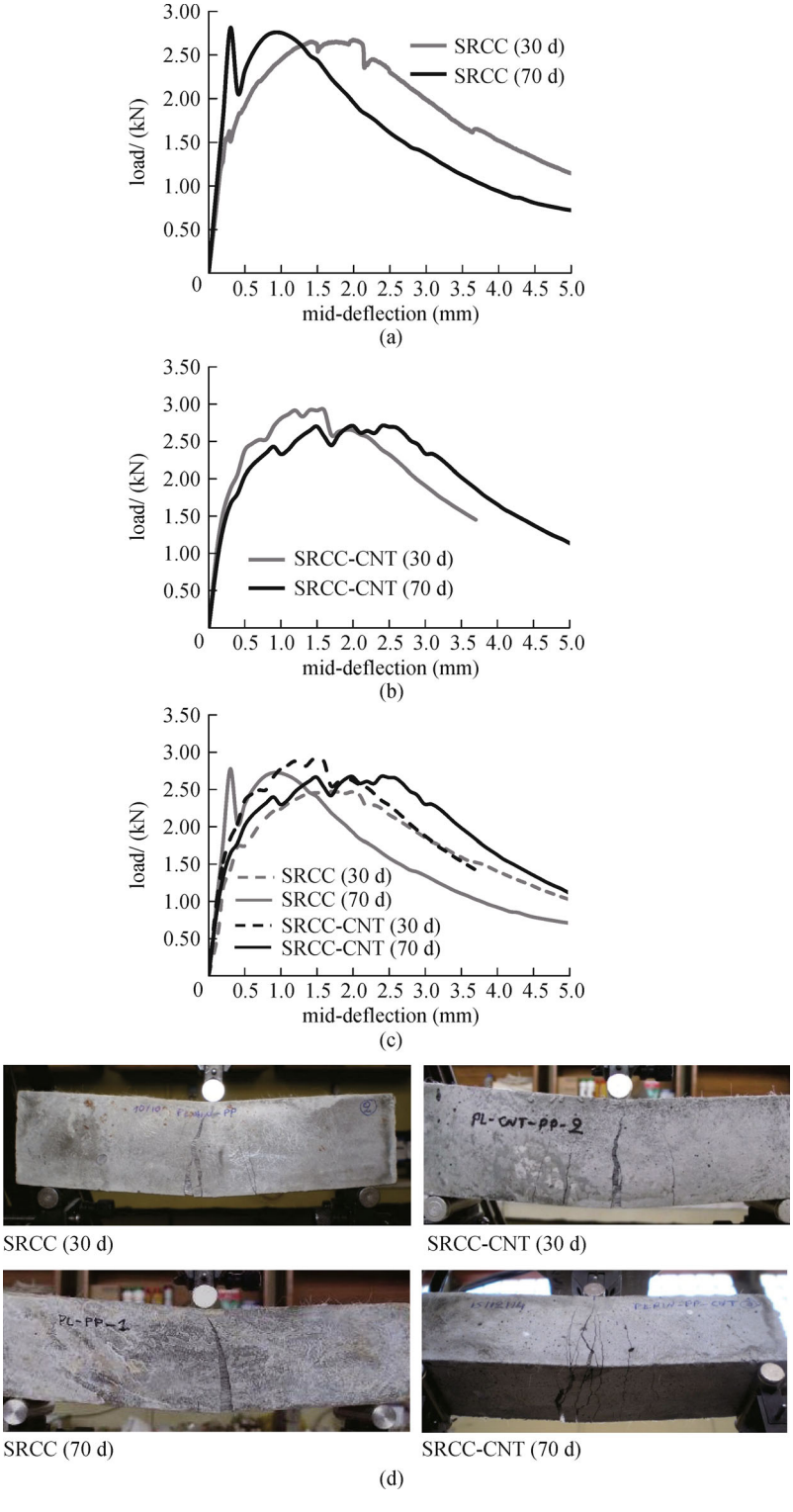

Fig. 5 SRCC and SRCC-CNT matrices: (a-b) average load — mid deflection responses of the 3-point bending tests on prisms, (c) comparative representation of the average envelopes of both matrices at both ages and (d) the associated failure patterns at both ages. (within brackets is the testing age in days)

the mix whereby crack opening occurred due to fibers' elongation rather than pullout, leading to a severe localization of all deformation in a single crack. Even in this case, the deflection capacity attained by the SRCC matrix (up to 15% loss of strength, i.e., at 85% of the peak residual load capacity) was about 10 times more than the value of the control (compare the grey continuous curves in Figs. 4(a) and 5(c)).

(iii) Investigating the SRCC-CNT matrix (black dashed and continuous curves in Fig. 5(c) and snapshots at right in Fig. 5(d)) the addition of the CNTs contributes towards the maintenance of the multi-cracking effect with time (tests conducted at 30th and 70th days of casting): the CNTs contribute to the development of multiple cracking and crack width control thus delaying or even postponing crack localization, beyond which the fibers' elongation rather debonding occurs. Studying the synergy of the PP fibers with the CNTs, the SRCC and SRCC-CNT matrices are compared (see the continuous curves in Fig. 5(c)): clearly the addition of CNTs succeeded in improvement of the apparent flexural toughness (in Fig. 5(c) the area under the SRCC-CNT (70 d) curve is larger than the SRCC (70 d)) and the pronounced deflection ductility (for up to 15% loss of strength, the SRCC-CNT (70 d) attained mid-deflection 3 mm as compared to the 1.5 mm of the SRCC (70 d)) regardless of testing time.

All experimental results of the studied matrices, as discussed above, are tabulated in Table 2, with reference to the three milestone stages of the load versus mid-deflection envelope: when apparent first cracking occurs (first drop of load), at strength (peak load) and at ultimate where 15% loss of strength has occurred.

After the flexural tests the two fractured parts of the prisms in the case of the control and the control with CNTs batches or the intact parts of the shear spans of the SRCC and SRCC-CNT batches were subjected to axial compression. In most cases six compression tests were performed for each batch, where the tested effective volume was a cube of 40 mm × 40 mm × 40 mm. The incorporation of CNTs both in control and SRCC matrices did not affect the compressive strength which was experimentally defined in the order of 60 MPa. This magnitude is only indicative because neither the size nor the aspect ratio (height/section size) are standard for the characterization of this property.

3 Bond specimens

3.1 Fabrication

A novel bond test setup was introduced for investigating the local bond-slip characteristics of steel reinforcement in ductile cementitious composite matrices. Twelve short beams of dimensions 370 mm × 80 mm × 70 mm (length × height × width) were casted, three identical coupons for each of the four studied batches. The beams were loaded under 4-point bending with the bonded length L_b being developed in the half of the mid-span of the constant moment region, and also in the tensile region of the cross section (Fig. 6(a)). Thus both the interactive materials (matrix and bar) were stressed in tension, succeeding in the objective to engage their tensile properties in developing the local bond — slip law. The bonded length was set equal to five times the bar diameter (i.e., $L_b = 5D_b$, where D_b = 10mm) with a clear bottom cover of 20 mm (= $2D_b$). The main bar of yielding stress f_{sy} = 500 MPa and Modulus of Elasticity E_s = 200 GPa (S500) was fully bonded in the left shear span whereas it was covered by a sleeve along the right one aiming to eliminate the bond interaction in that region (Figs. 6(b,c)). Because the right shear span was actually "unreinforced", flexural strength as required by the moment diagram in that region was achieved by using two auxiliary longitudinal bars of 8mm (S500 also). These bars were fully bonded along the right shear span and lap-spliced along the studied bonded length. In designing the specimens, the aim was to preclude all the other possible and premature modes of failure apart from bond failure which was the study objective. A preformed 20 mm wide groove was located just to the left of midspan of the beam specimen, extending across the width and up to a distance of 2.5D_b from the tension face. The groove was necessary so as to control the magnitude of bar maximum tensile force which may be quantified through sectional analysis of the mid-cross section.

Table 2 Experimental average values for applied force and mid deflection at milestones (apparent first cracking-subscript *y*, peak-subscript *u* and ultimate-subscript u.85%) and analytical estimations of tensile indices (apparent flexural toughness G_f and modulus of Rupture $f_{t,fl}$ as per [13])

Matrix ID – (age in days)	experimental results					tensile indices	
	Δ_y (mm)	Δ_u(mm)	$\Delta_{u.\ 85\%}$ (mm)	P_y (kN)	P_u (kN)	G_f (Nt·m^{-1})	$f_{t,fl}$ (MPa)
Control (70 d)	0.16	0.16	0.16	1.45	1.45	73	4.75
Control –CNT (30 d)	0.23	0.23	0.23	2.39	2.39	172	7.83
SRCC (30 d)	0.28	1.80	2.62	1.55	2.53	3275	5.10
SRCC(70 d)	0.28	0.93	1.47	2.70	2.36	1997	8.86
SRCC-CNT (30 d)	0.18	1.56	2.25	1.66	3.01	3307	5.43
SRCC-CNT (70 d)	0.27	2.21	3.01	1.66	2.84	4193	5.46

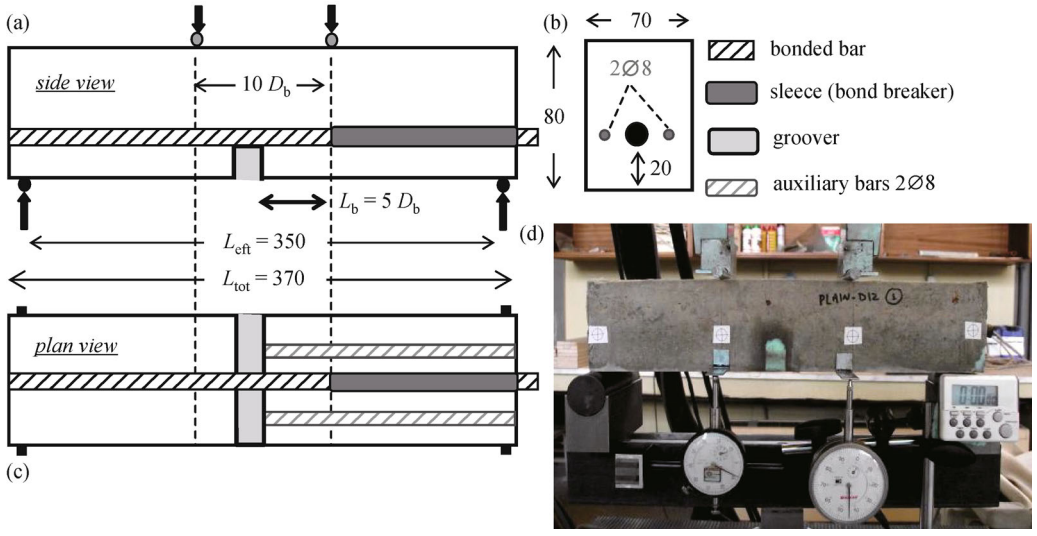

Fig. 6 (a,b) Geometry and (c) detailing of the 4-point bending short beam for investigation of local bond in the constant moment region. (d) Setup and instrumentation of the specimens

Tests were conducted using a protocol for displacement control with a loading rate of 0.2 mm/min up to the attainment of the first peak and then of 0.5mm/min up to test termination. Figure 6(d) illustrates the test setup and the instrumentation of the specimens.

3.2 Experimental results

Figure 7(a) depicts the applied load versus mid deflection average envelopes of all the bond tests for the SRCC and SRCC-CNT tests. The response average curves of each subgroup are discussed here, aiming to examine the structural performance of bond, where the two materials collaborated. The following observations are drawn:

(i) With reference to the control matrices there is a slight increase of the initial stiffness and a milder slope of the descending branch after peak due to the addition of the CNTs (in Fig. 7(a), compare the black with the grey curves respectively). The earlier testing time of the control-CNT matrix resulted in similar strengths of the control matrices. Strength was expected to be increased with time, and for this reason additional control-CNT specimens were scheduled to be constructed for testing at a later age. The aforementioned increase of matrix strength due to CNTs (see Fig. 4(a)) was not manifested in the corresponding bond tests, probably obscured by the dominating influence of steel reinforcement in the load-carrying capacity of the specimens.

(ii) With reference to the SRCC matrices, the addition of the PP fibers resulted in an impressive increase of both the strength and displacement ductility (threefold and tenfold respectively the values of the control and the control with CNTs batches, see the dashed grey curve in Fig. 7(a)), with the latter property being improved due to the addition of the CNTs, see the dashed black curve in Fig. 7(a) (this is also evident in the relevant matrix tests of Fig. 5(c)).

(iii) The notable ductile response of all the SRCC and SRCC-CNT bond tests (Fig. 7(a)), where no loss of load carrying capacity occurs with increased deflection, is not a result of yielding of the reinforcing bars: the theoretical bar yielding load was calculated as P_{yield} = 31 kN (i.e., this load value, after applying sectional analysis, corresponds to the yielding bar stress of 500 MPa), much greater than the ultimate load attained by any of the short anchorage bond tests of this study. Rather, the ductile response is attributable to the sustained lateral pressure exerted by the cover on the bar's lateral surface, while the bar translated from its surroundings; this lateral pressure was possible because of the resilience of the cover to hoop-tension and was due to confining effect provided by the synergistic action of the CNTs and the PP fibers.

(iv) Figure 7(b) shows the cracking pattern that was developed on the lateral face of all the bond tests near failure. Controlled bar pullout under sustained load was evident in the case of the SRCC and nano/fiber (SRCC-CNT) reinforced specimens with a multi-cracking network with large deformations in the region where bond was studied as compared with the single large crack of the control and the nano (control-CNT) reinforced specimens, accompanied with instant cover splitting. Note that bottom cover splitting over the test-bar occurred in all bond tests (see Fig. 7(c)), at peak load for the control bond tests and at advanced deformation for the SRCC and SRCC-CNT bond tests.

From the available experimental bond results it may be concluded that the use of CNTs not only increases the toughness of the matrix (ascending slope-cases control and control-CNT, and strength-cases SRCC and SRCC-CNT, all in Fig. 7(a)) but also influences the interfacial bond of fiber-to-matrix and bar development capacity thus achiev-

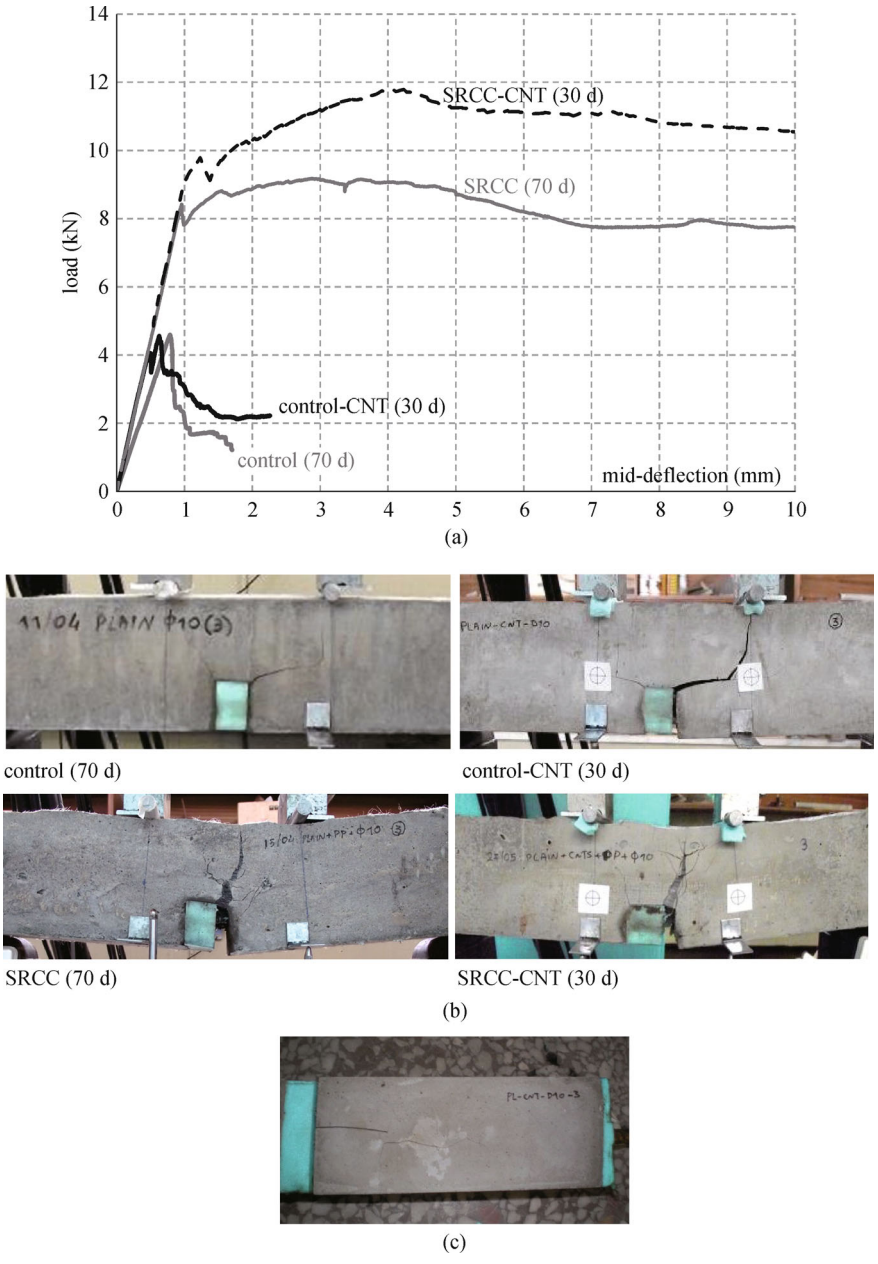

Fig. 7 (a) Average load — mid deflection responses of the bond tests. (b) Cracking pattern near failure on the lateral face of all bond tests. (c) Splitting cracking of the bottom cover along the bonded length occurred in every case

ing the multi-cracking effect at advanced aging. Regarding the age of testing and its effects on resilience (i.e., on sustained ductile response) — particularly for the subgroup SRCC-CNT, further experimental documentation is deemed necessary.

These bond test data (applied load versus mid-deflection envelopes) will be used for the extraction of the local bond-slip law, as follows: (i) the bond stress will be extracted from the applied load, by implementing moment and force equilibrium equations, and (ii) the slip values will be extracted from the displacement records by implementing equations of virtual work. Thus, in the ongoing work, the objective is being extended to extract and parameterize the properties of a local bond-slip law for reinforcing bars anchored in CNT-enhanced SRCCs, which is pre-requisite to implementation of these materials in structural components.

4 Conclusions

The prospects of the emerging strain-resilient cementitious composites in construction depends to a large extent on its efficacy as a host matrix for structural steel reinforcement.

In the present study bond of reinforcing bars embedded in an innovative cementitious matrix was the motivating objective. To build understanding and experimental evidence in this front, the experimental program consist of two phases: the first phase was concerned with characterization of the tensile response of the basic cementitious matrix, with improvements imparted by the addition of combinations of fibers including carbon nanotubes and synthetic fibers (Polypropylene). In the second phase reinforcing bar development (through bond) was studied in order to determine the resilience of these matrices and their efficacy in supporting development of the bar stress to large levels of pullout-slip. Tests were conducted in the laboratory of Applied Mechanics of DUTh. The aim of the research was to highlight the tensile strength improvement and the magnitude of absorbed energy (the latter is described by the area under the load — deflection history and the abscissa of deflections) and displacement ductility amplitude with reference to the age of testing, which strongly affects the matrix-to-fiber bond interaction.

The basic findings from the material characterization phase were as follows: (i) the CNTs in a dosage of 0.1% per weight of cement, in the control matrix (without PP fibers) induce a strength increase by as much as 65% and an apparent flexural toughness increase by 138% (form 73 to 172 $Nt \cdot m^{-1}$, Table 2) over the plain mix (containing no CNTs). (ii) In the SRCC matrix, the addition of the PP fibers results in improvement of both the strength and displacement ductility, with the latter being compromised with age. (iii) The addition of CNTs in SRCC maintains the multicracking effect with time (i.e., the ability of the material to develop a broad process zone in tension rather than concentrating all deformation in a single location). In this hybrid CNT-PP mix, the CNTs contribute to the development of multiple cracking and crack width control. Comparing the synergy of the PP fibers with the CNTs, the latter are deemed responsible for doubling the already enormously increased flexural toughness (at later age, from 73 for the Control, to 1997 for the SRCC, to 4193 $Nt \cdot m^{-1}$ for the SRCC-CNT, Table 2) due to the maintenance of displacement ductility and to milder slope of the post-peak descending branch of the load-displacement response curves.

The basic findings from the structural tests on local bond mechanism of steel reinforcement to hybrid SRCC-CNT matrix were as follows: (i) the addition of PP fibers resulted in an impressive increase of both the load carrying capacity and displacement ductility (threefold and tenfold increase, respectively, as compared to the values of the control matrices), with the ductility being improved due to the addition of the CNTs. The notably ductile response of all the SRCC bond tests under sustained load (i.e., with no loss of load carrying capacity), is not a result of bar yielding as one would surmise from the appearance of the load-displacement curves, but it is owing to controlled sliding of the bar from its surroundings due to the confinement provided by the synergistic action of the CNTs and the PP fibers. (ii) The controlled sliding in the case of the SRCC-CNT bond tests results in a multi-cracking network with large deformations in the region where bond is studied. (iii) Regarding the age of testing and its effects on the ductile behavior (especially for the subgroup SRCC-CNT that was tested only at an early age) further experimentation is deemed as an important future research need.

Acknowledgements Funding for this investigation is provided by the research project "Thalis—DUTh. Center for Multifunctional Nano-Composite Construction Materials" sponsored by the European Social Fund & the Greek National Strategic Reference Framework (NSRF) 2007−2013. The help provided by the Ph.D. candidates of the Lab. of Applied Mechanics of DUTh, P. Danoglidis, M. Katotriotou and M. Falara is greatly appreciated.

References

1. Tastani S P, Pantazopoulou S J. Direct tension pullout bond test: experimental results. ASCE Structural Engineering, 2010, 136(6): 731–743
2. Tastani S P, Pantazopoulou S J. Reinforcement and concrete bond: state determination along the development length. Journal of Structural Engineering, 2013, 139(9): 1567–1581
3. Fischer G, Li V C. Effect of matrix ductility on deformation behavior of steel-reinforced ECC flexural membersunder reversed cyclic loading conditions. ACI Structural Journal, 2002, 99(6): 781–790
4. Bandelt M J, Billington S L. Bond behavior of steel reinforcement in high-performancefiber-reinforced cementitious composite flexural members. Materials and Structures, 2016, 49(1-2): 71–86
5. Bandelt M J, Billington S L. Monotonic and cyclic bond-slip behavior of ductile high-performance fiber-reinforced cement-based composites. In: Proceedings of the 3rd International. RILEM Conference on Strain Hardening Cementitious Composites, Dordrecht Netherlands, November 3−5, 2014, 393–400
6. Konsta-Gdoutos M S, Metaxa Z S, Shah S P. Multi-scale mechanical and fracture characteristics and early-age strain capacity of high performance carbon nanotube/cement nanocomposites. Elsevier Cement & Concrete Composites, 2010, 32(2): 110–115
7. Metaxa Z S, Konsta-Gdoutos M S, Shah S P. Mechanical properties and nanostructure of cement-based materials reinforced with carbon nanofibers and polyvinyl alcohol (PVA) microfibers. Advances in the Material Science of Concrete, 2010, 270: 115–124
8. Chao S H, Naaman A E, Parra-Montesinos G J. Bond behavior of reinforcing bars in tensile strain-hardening fiber-reinforced cement composites. ACI Structural Journal, 2009, 106(6): 897–906
9. Georgiou A V, Pantazopoulou S J, Petrou M F. Experimental analysis of fiber reinforced cementitious composites with increased toughness. In: Proceedings of the 10th HSTAM International Congress on Mechanics, Chania, Greece, 25–27 May, 2013
10. Georgiou A V, Pantazopoulou S J. Bond, crack-width estimation, crack spacing and effective material stiffness in strain hardening cementitious composites. In: Proceedings ofthe SHCC3-3rd Inter-

national RILEM Conference on Strain Hardening Cementitious Composites, 3−5 November, 2014, Dordrecht, the Netherlands

11. Konsta-Gdoutos M S, Metaxa Z S, Shah S P. Highly dispersed carbon nanotube reinforced cement based materials. Elsevier Cement and Concrete Research, 2010, 40(7): 1052–1059
12. Hersam M C, Seo J W T, Shah S P, Konsta-Gdoutos M S, Metaxa Z S. Highly Concentrated Nano-Reinforcement Suspensions for Cementitious Materials and Method of Reinforcing Such Materials. US Patent, 2011
13. ASTM C293-94. Standard Test Method for Flexural Strength of Concrete (Using Simple Beam with Center-Point Loading). ASTM International, West Conshohocken, PA, USA, 2002